Structure, Morphology and Opto-Electrical Properties of Nanostructured Indium Doped SnO_2 Thin Films Deposited by Thermal Evaporation

Md. Mahafuzur Rahaman
University of Dhaka, Dhaka, Bangladesh
Kazi Md. Amjad Hussain
Atomic Energy Center, Dhaka, Bangladesh
Mehnaz Sharmin
Bangladesh University of Engineering and Technology, Dhaka, Bangladesh
Chitra Das
BRAC University, Dhaka, Bangladesh
Shamima Choudhury, Prof.
University of Dhaka, Dhaka, Bangladesh

doi: 10.19044/esj.2016.v12n27p263 URL:http://dx.doi.org/10.19044/esj.2016.v12n27p263

Abstract

Indium doped Tin oxide (SnO_2: In) thin films of various thicknesses (200-600 nm) with fixed 2% indium (In) concentration were prepared by thermal evaporation method onto glass substrates under high vacuum (10^{-6} Torr). As deposited films were vacuum annealed at 200^o C for 60 minutes. The structure, optical, electrical and morphology properties of SnO_2: In thin films were investigated as a function of film thickness. The XRD analysis revealed that films were polycrystalline in nature with a tetragonal structure having (110) plane as the preferred orientation. The average crystalline size increased from 34.8 to 51.25 nm with increase of film thicknesses. The surface morphology of the doped films was obtained by Atomic Force Microscopy (AFM) and Field Emission Scanning Electron Microscopy (FESEM). Optical transmittance was obtained from a double beam UV-Vis-NIR spectrophotometer. Maximum transmittance varied from 65-76% in the visible range of the spectrum. Optical band gap (E_g) varied between 2.89 and 3.20 eV. The resistivity of SnO_2: In thin films was as high as 10^5 Ω-cm. Activation energy of the films were found to be 0.18 to 0.47 eV for 300-600 nm film thicknesses. Due to high optical band gap and high electrical resistivity, these nanostructured films can be used in optoelectronic devices especially as opto-isolator.

Keywords: Nanostructured films, XRD, AFM, FESEM, Band gap

Introduction

Tin oxide (SnO_2) is a wide band gap (3.6 eV) n-type semiconductor where oxygen vacancies act as n-type dopants (Batzil, 2005). SnO_2 films have attractive properties like high transmittance in the visible range, low resistivity and thermal stability (Zadsar, 2012) for which it has immense applications such as gas sensing material for photovoltaic cell (Cachet, 1997), gas sensors devices (Galdikas, 1997), window materials in solar cells (Roy, 2010), transparent conductive electrode for solar cells (Mohammadi-Gheidani, 2005) and so on. Pure and doped-SnO_2 thin films can be prepared by various techniques, such as sol-gel (Banerjee, 2003), spray pyrolysis (Gokulakrisshan, 2011), electron beam evaporation (Shamala, 2004), electrostatic spray deposition (Joshi, 2013), RF sputtering (Tuna, 2010) and thermal evaporation (Chuhan, 2012). Among these methods, vacuum evaporation has the advantages of depositing high purity crystalline and uniform films in a single step. This method is substrate friendly and materials can be deposited in short time.

P-type SnO_2 can be fabricated with effective substitution of Sn with group III-family elements such as aluminum (Al), gallium (Ga), indium (In). Recently there have been a number of studies on group III elements doped SnO_2 thin films such as Al doped SnO_2 (Ahmed, 2006; Bagheri-Mohagheghi, 2004), Ga doped SnO_2 (Yang, 2010), SnO_2: In (Chowdhury, 2011; Ji, 2006). We had investigated the optical properties of Indium doped tin oxide thin films with various concentration of indium at a fixed thickness of 200 nm by thermal evaporation method (Chowdhury, 2011).

In this present work, indium doped tin oxide thin films were prepared with varying thicknesses (200-600 nm) and the prepared thin films were vacuum annealed at 200°C for 60 minutes. The effects of film thickness on the structure, optical, electrical and morphology properties were investigated.

Experimental

SnO_2: In thin films were deposited on to glass substrates by thermal evaporation method using a vacuum evaporation unit (EU-300), in high vacuum (~10^{-6}Torr). Two molybdenum boats- one for Indium and another for SnO_2- were used as a resistively heated source for the evaporation. The substrate was placed at a distance 6.4 cm above the source materials. Before deposition, glass substrates were cleaned chemically and ultrasonically. The rate of evaporation was 0.2 nm/sec measured *in situ* by the FTM5 quartz crystal thickness monitor (Edwards, UK). Thin films of various thicknesses (200, 300, 400, 500 and 600 nm) were prepared keeping substrate temperature constant at 100°C. As deposited films were vacuum annealed at

200°C for 60 minutes. The structure of the SnO_2: In thin films was examined by X-Ray diffraction (XRD) measurements using PHILIPS PW 3040 X' Pert PRO system. The surface morphology of the films was performed using Atomic Force Microscope (AFM) (Nano Surf) and Field Emission Scanning Electron Microscope (FESEM) of model JEOL JSM-7600F. A double beam UV-VIS-NIR recording spectrophotometer (Shimadzu, UV-3100) was used to measure optical transmittance (T%) and reflectance (R%) of the SnO_2: In thin films. The resistivity of the films was measured by locally fabricated four point probe method. Resistivity of the films were studied in the temperature range 25°C-100°C and activation energy was calculated from the obtained data.

Results and Discussion

Structural Analysis

Typical XRD patterns of the annealed indium doped tin oxide thin films of different thicknesses are shown in Figure 1. All the films are oriented along (110) direction and the peak position is consistent with the JCPDS file card No. 41-1445, which is in agreement with the other workers (Gurakar, 2014). The intensity of the (110) diffraction peak increases with film thickness. Thin film of 200 nm is less crystalline due to the effect of amorphous glass substrate. The effect of the glass substrate decreases with the increase of film thickness. The crystallinity of the films increases with film thickness up to 500 nm.

There is no peak for indium oxide, indicating that indium incorporates into SnO_2 lattice. Form Table 1 it can be shown that diffraction angle decreases with the increase of film thicknesses. The decrease in diffraction angle results in increase of the lattice constants due to the larger size of In^{3+} (0.81 Å) compared to Sn^{4+} (0.71 Å). This is an indication of increase of substitution of Sn^{4+} by $In^{3+}$with the film thickness (Ji, 2006).

The average size of the crystallites (D) corresponding to (110) direction was calculated using the Scherrer's formula (Cullity, 1972)

$$D = \frac{0.9\lambda}{\beta \cos\theta} \qquad (1)$$

Where, λ is the wavelength of the X-rays, β is the full width at half maxima (FWHM) of the peak which has maximum intensity, and θ is the Bragg's angle. The variation of crystallite size with film thickness is shown in Table. 1. It is clear from the table that crystallite size increases with increasing film thickness.

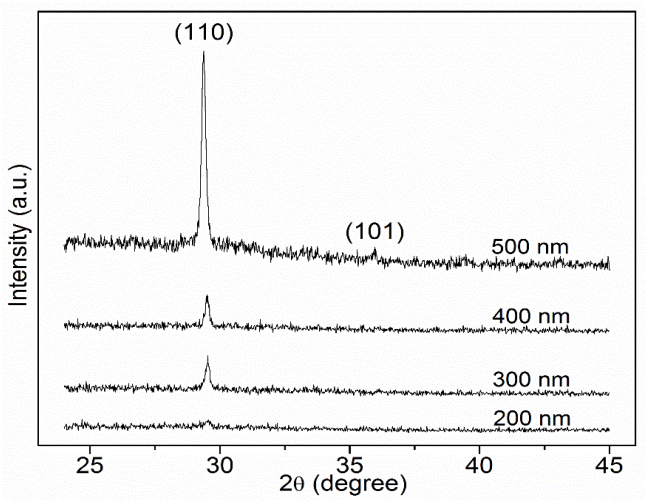

Figure 1: XRD patterns of SnO_2: In thin films of different thicknesses.

The dislocation density (δ) and the strain (ε) of the films were determined with the use of the following formula (Jassim, 2013)

$$\delta = {}^{1}/_{D^2} \qquad (2)$$

$$\epsilon = \frac{\beta \cos\theta}{4} \qquad (3)$$

Where, δ is defined as the length of dislocation lines per unit volume. It is the measure of the amount of defects in a crystal. The dependence of the strain and dislocation density of SnO_2: In thin films on thickness is shown in Table 1.

It is seen from Table. 1, that strain and dislocation density decrease with the increase of film thickness. This decrease in strain and dislocation density indicates a decrease in the concentration of lattice imperfection.

Table 1: Structural properties of SnO_2: In thin films of different thicknesses

Thickness (nm)	Plane	Position 2θ°	Distance between crystal plane, d (Å)	Cryst-allite Size, D (nm)	Dislocation Density, δ (cm^{-2})	Microstrain ε
200	(110)	29.55	3.0205	34.80	8.26×10^{10}	9.97×10^{-5}
300		29.53	3.0225	45.83	4.76×10^{10}	7.56×10^{-5}
400		29.51	3.0245	47.03	4.52×10^{10}	7.37×10^{-5}
500		29.38	3.0376	51.25	3.81×10^{10}	6.54×10^{-4}

Optical Properties

The variation of optical transmittance (T %) and reflectance (R %) of the indium doped tin oxide thin films were measured with photon wavelength in the range of 300-2500 nm. Figure 2 shows T% and R% spectra of the films at different film thicknesses. The spectra shows

interference pattern with a sudden fall of transmittance near the band edge. The maximum transmittance of the films varies from 65% to 76% in the visible range of spectrum. All the films show maximum transmittance in NIR region and peaks of transmittance spectrum shift towards the higher wavelength with film thicknesses. The 300nm doped film shows maximum transmission (85%) in NIR region. Das *et al.* found similar results for vacuum evaporated GaAs thin films. The reflectance spectra shows interference pattern with distinct peaks and valleys.

Extinction coefficient (k) was obtained from Transmission (T%) and Reflection (R%) measurements (Heavens, 1955 and Tomlin, 1968). For a film of thickness d which has a complex refractive index, n_1-ik_1, the relevant equations are

$$\frac{1}{4n_2(n_1^2+k_1^2)}\begin{bmatrix}(1+n_1^2+k_1^2)\{(n_1^2+n_2^2+k_1^2)\cosh 2\alpha_1+2n_1n_2\sinh 2\alpha_1\}+\\(1-n_1^2-k_1^2)\{(n_1^2-n_2^2+k_1^2)\cos 2\gamma_1-2n_2k_1\sin 2\gamma_1\}\end{bmatrix}-\frac{1+R}{T}=f_1(n_1,k_1)=0 \quad (4)$$

$$\frac{1}{2n_2(n_1^2+k_1^2)}\begin{bmatrix}n_1\{(n_1^2+n_2^2+k_1^2)\sinh 2\alpha_1+2n_1n_2\cosh 2\alpha_1\}+\\k_1\{(n_1^2-n_2^2+k_1^2)\sin 2\gamma_1+2n_2k_1\cos 2\gamma_1\}\end{bmatrix}-\frac{1-R}{T}=f_2(n_1,k_1)=0 \quad (5)$$

Where, n_1=2.006 and n_2=1.45 are refractive indices of the films and substrate, respectively. k_1 is the extinction-coefficient of the films. $\alpha_1=\frac{2\pi k_1 d}{\lambda}$ and $\gamma_1=\frac{(2\pi n_1 d)}{\lambda}$, where λ is the wavelength of light. For each value of n_1, a value of k_1 is computed from Eq. (5). This value is then fed into Eq. (6) to determine the condition $f_2(n_1,k_1)\cong 0$. The procedure is repeated until the best solution is found.

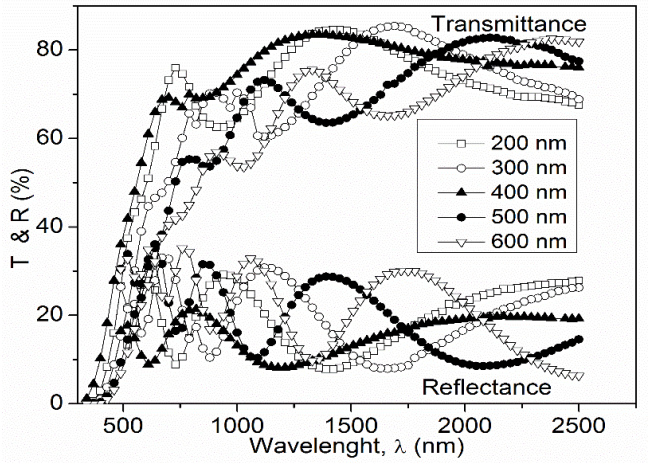

Figure 2: Optical transmittance T (%) and reflectance R (%) versus wavelength (λ) of SnO_2: In films at different thicknesses.

Dependence of extinction coefficient with wavelength is represented in Figure 3. Extinction co-efficient exhibits very high value near UV region indicating high absorption in that wavelength region and begins to decrease as the wavelength increases and seems to be saturated in the visible and infrared region. It is also observed that the highest value of the extinction co-efficient decreases with the increase of film thickness. Similar results was observed for vacuum evaporated CdTe thin films (Mousumi, 2014).

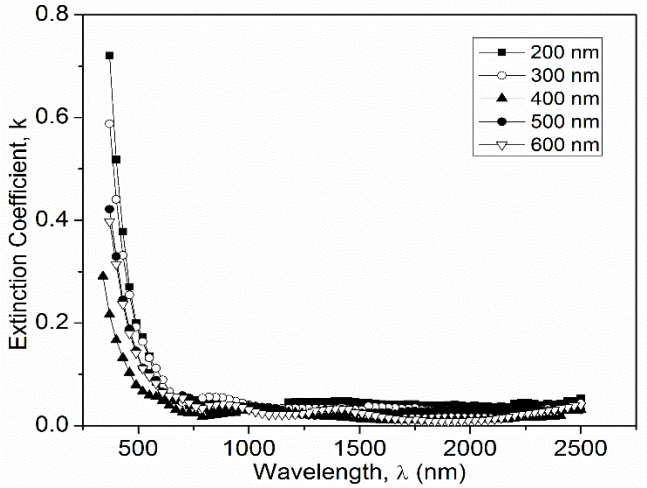

Figure 3: Variation of extinction co-efficient (k) with wavelength (λ) for SnO_2:In thin films of different thicknesses.

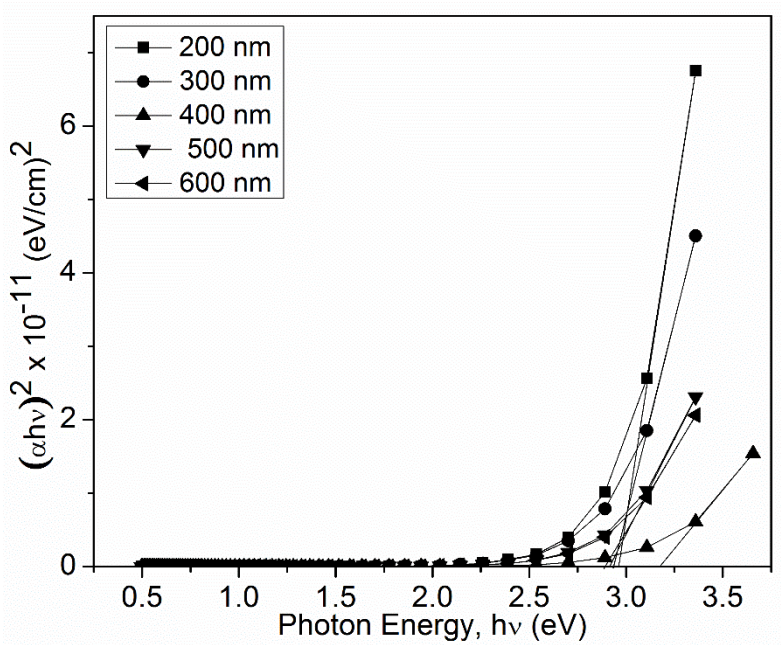

Figure 4: Dependence of $(\alpha h\nu)^2$ on incident photon energy ($h\nu$) for SnO_2: In thin films for different thicknesses.

Figure 4 shows a plot of $(\alpha h\nu)^2$versus photon energy ($h\nu$) for SnO_2: In thin films of different thickness. The values of the direct optical band gap E_g were determined by extrapolations of the linear regions of the plots to zero absorption ($\alpha h\nu = 0$).

Optical band gap of films is depicted in Figure 5. The 300nm film shows minimum band gap. A shift in optical band gap is observed from 2.89 eV to 3.20 eV as the film thickness increases from 300 nm to 400 nm. The shift of band gap towards higher energy can be explained by the Burstein-Moss shift. The dependence of B-M shift with thickness was observed by Kim *et al.* for the thickness varying indium-tin-oxide thin films. These band gap values are in agreement with the band gap values of concentration varying Indium doped SnO_2 films (2.77 - 2.98 eV) deposited on glass substrate using thermal evaporation method (Chowdhury, 2011).

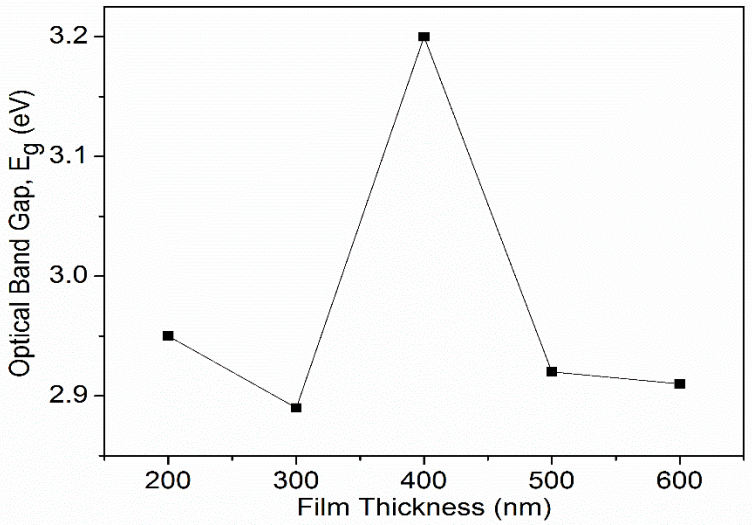

Figure 5: Dependence of optical band gap (E_g) on film thickness of SnO_2: In thin films.

Electrical Properties

Figure 6 shows plot of resistivity as a function of film thickness for SnO_2: In films. The films reveal a high resistivity which varies in between 1.5 x 10^5 and 3.6 x 10^5 Ω-cm. These results are in agreement with the works reported by (Benouis, 2011 and Ji, 2003). Substitution of tin (Sn^{4+}) tetravalent by trivalent indium (In^{3+}) may cause a deficiency of one electron or creation of a hole which results in increasing the resistivity of films.

The resistivity of the SnO_2: In films increases with the film thickness upto 500 nm. There are may be two reasons for the increase of resistivity. (i) From XRD spectra it is observed that, the substitution of Sn^{4+} by In^{3+} increases with the film thickness which decreases the n-type carrier concentration. (ii) The increase in resistivity may be due to the increase in grain size with film thickness. Because the incorporation of indium may take

place at the grain boundary which can decrease the carrier concentration resulting in increasing the resistivity (Pe Waal, 1981).

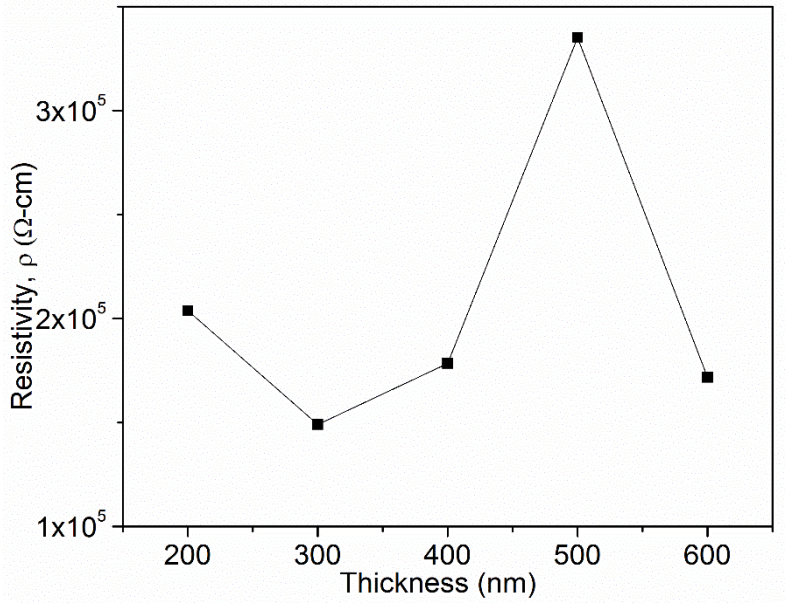

Figure 6: Dependence of electrical resistivity (ρ) as a function of film thickness for SnO_2: In films deposited at T_s= 100 ^oC.

The electrical conductivity(σ) against temperature is expressed as follows (Chopra, 1969),

$$\sigma = \sigma_0 \exp\left(-\frac{\Delta E}{2kT}\right) \qquad (7)$$

Where, ΔE is the thermal activation energy, $\sigma_0$is the conductivity at T = 0 K, k is the Boltzmann constant.

The inset of Figure 7 shows the dependence of thermal activation energy ΔE (eV) on the thickness of SnO_2: In thin films. The straight line nature of Arrhenius plot indicates the thermally activated conduction which often found in doped semiconductors. ΔE varies between 0.18 to 0.47 eV with film thickness which is larger than those found by (Benouis, 2011) for spray pyrolysis SnO_2: In thin films. The inset of Figure 7 shows that 500 nm thin film has maximum activation energy. As 500 nm SnO_2: In film has the largest grain size, maximum energy is needed to transfer a charge from one grain to another grain.

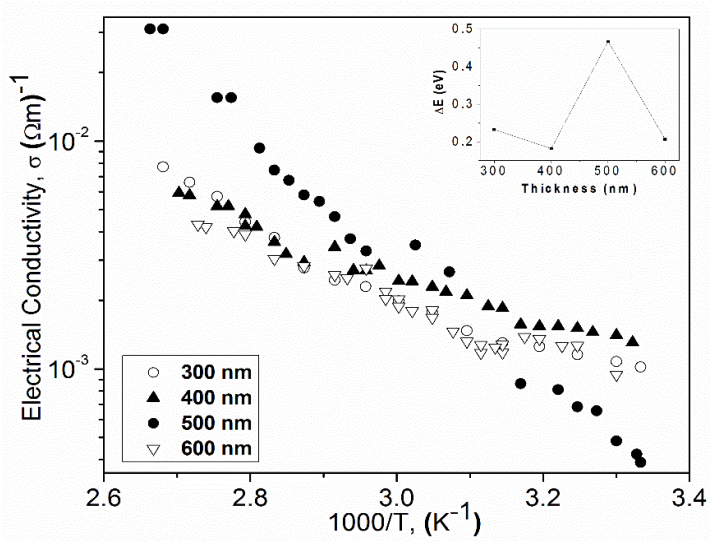

Figure 7: Semi-log plot of electrical conductivity (σ), inset shows profile of activation energy (ΔE) dependence on film thickness.

Surface Morphology and Elemental Analysis

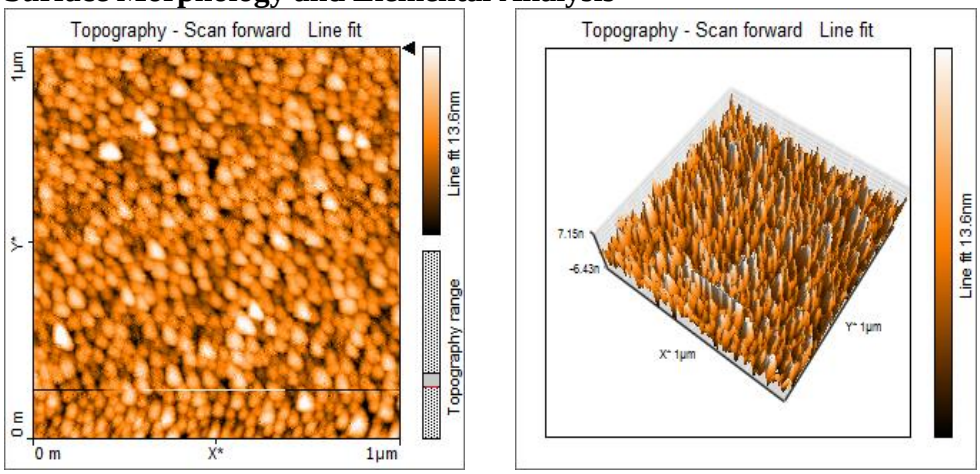

(a) **(b)**

Figure 8: Atomic Force Micrograph (AFM) of the surface of SnO_2: In film of thickness 300 nm deposited by thermal evaporation method (a) 2D view, (b) 3D view.

Figure 8 shows AFM image (1µm x 1µm) of SnO_2: In thin film with thickness 300 nm. It is observed that the distribution of grains is uniform on the surface. The root-mean-square (rms) surface roughness of the film is 2.98 nm. Average crystallite size of the film is 42.87 nm which is in consistence with the XRD data of the film.

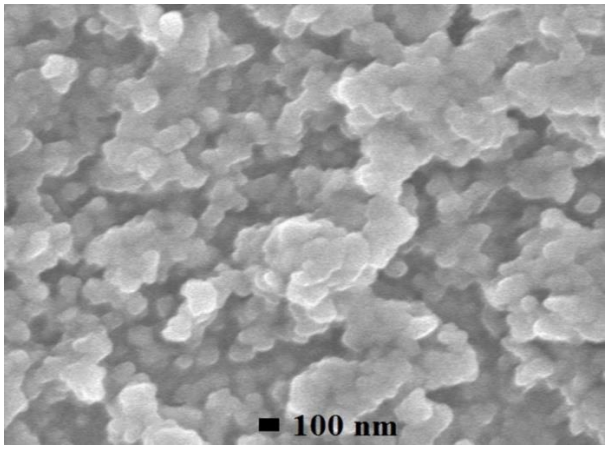

Figure 9: SEM image (x 30K) shows the surface morphology of the SnO_2: In film of thickness 300 nm.

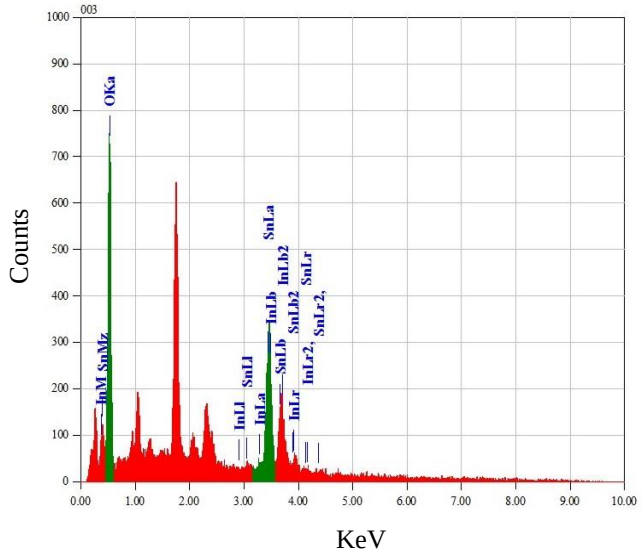

Figure 10: EDX image of SnO_2: In thin film of thickness 300 nm.

The SEM surface view of the SnO_2: In film of thickness 300 nm is shown in Figure 9. The SEM micrograph shows small crystallites and agglomeration of the grain particles for the film. Energy Dispersive X-ray (EDX) spectra of indium doped tin oxide thin film shows that the grains are comprised of O, Sn and In. EDX spectrum is shown in Figure 10. Atomic% of Sn, O and In were found as 13.27, 85.23 and 1.50 respectively. Stoichiometry of this film is confirmed by EDX data.

Conclusion

The role of film thickness on structure, optical, electrical and morphology properties of vacuum evaporated In doped SnO_2 thin films were studied in this present research work. XRD measurement reveals the tetragonal structure with the dominant peak (110). Here crystallinity increases with film thicknesses up to 500 nm. These thin films are highly transparent in NIR region. Maximum transmittance (85%), lowest optical band gap (2.89 eV) is obtained for the film of thickness 300 nm. High electrical resistivity is observed for SnO_2: In thin films and least value of resistivity is found for 300 nm thickness. SEM and AFM micrographs reveals homogeneous surface of the film with rms surface roughness 2.98 nm. Due to high optical band gap and high resistivity, SnO_2: In thin films can be used in different optoelectronic devices especially as opto-isolator.

Acknowledgements

Laboratory facilities of Experimental Physics Division, Atomic Energy Centre, Dhaka; Department of Physics, University of Dhaka; Centre for Advanced Research in Sciences (CARS), University of Dhaka; Department of Physics, Bangladesh University of Engineering &Technology (BUET); Department of Glass & Ceramics, BUET; are acknowledged.

References:

Ahmed, S. F., Khan, S., Ghosh, P. K., Mitra, M. K., & Chattopadhyay, K. K. (2006). *Effect of Al doping on the conductivity type inversion and electro-optical properties of SnO2 thin films synthesized by sol-gel technique*. J. Technol., Vol. 39, pp. 241-247.

Bagheri-Mohagheghi, M.-M., & Shokooh-Saremi, M. (2004). *The influence of Al doping on the electrical, optical and structural properties of SnO_2 transparent conducting films deposited by the spray pyrolysis technique*. J. Phys. D: Appl. Phys., Vol. 37, pp. 1248-1253.

Banerjee, A. R., Kundo, S., Saha, P., & Chattopadhyay, K. K. (2003). *Synthesis and Characterization of Nano-Crystalline Fluorine-Doped Tin Oxide Thin Films by Sol-Gel Method*. Journal of Sol-Gel Science and Technology, Vol. 28, pp. 105-110.

Batzil, M., & Diebold, U. (2005). *The surface and materials science of tin oxide*. Progress in Surface Science, Vol. 79, pp. 47-154.

Benouis, C. E., Benhaliliba, M., Yakuphanoglu, F., Tiburcio Silver, A., Aidad, M.S., & Juareze, A. S. (2011). *Physical properties of ultrasonic sprayed nanosized indium doped SnO2 films*. Synthetic Metals, Vol. 161, pp. 1509– 1516.

Cachet, Bruneaux, J., Folcher, G., Levy- Clement, C., Vard, C. & Neumann-Spallart M. (1997). *n-Si/SnO2 junctions based on macro porous silicon for photo conversion*. Solar Energy mater and Solar Cells, Vol. 46, pp. 10-1141.
Chopra, K. L. (1969). *Thin Film Phenomena*. McGraw-Hill, New York, NY, USA.
Chowdhury, F. R., Choudhury, S., Hasan, F., & Begum, T. (2011). *Optical properties of undoped and indium doped tin oxide thin films*. J. Bangladesh Acad. Sci., Vol. 35(1), pp. 99-111.
Chuhan, R. S., Kumar, V., Agarwal, D. C., Pratap, D., Sulania, I., & Tripathi, A. (2012). *SHI induced modifications in SnO_2 thin films: Structural, optical and surface morphological studies*. Nuclear Instruments and Methods in Physics Research B, Vol. 286, pp. 295-298.
Cullity, B. D. (1972). *Elements of X-ray diffraction*. Reading, MA: Addison-Wesley.
Das, C., Begum, J., Begum, T., & Choudhury, S. (2013). *Effect of thickness on the optical properties of GaAs thin films*. J. Bangladesh Acad. Sci., Vol. 37(1), pp. 83-91.
Galdikas, A., Jasutis, V., Kaciulis, S., Mattogno, G., Mironas, A., Olevano, V., Senuliene D., & Setkus, A. (1997) *Pecularities of surface doping with Cu in SnO_2 thin film gas sensors*. Sensors and Actuators B, Vol. 43, pp. 140-146.
Gokulakrisshan, V., Parthiban, S., Jeganathan, K., & Ramamurthi, K. (2011). *Investigation on the structural, optical and electrical properties of Nb-doped SnO_2 thin films*. J Mater Sci, Vol. 46, pp. 5553-5558.
Gurakar, S., Serin, T. & Serin, N. (2014). *Electrical and microstructural properties of (Cu, Al, In)-doped SnO_2 films deposited by spray* pyrolysis. Advanced Materials Letters, Vol. 5(6), pp. 309-314.
Heavans, O. S. (1955). *Optical Properties of Thin Solid Films*. Butterworths Scientific Publications, London.
Jassim, S. A., Zumaila, A. A. R. A., & Waly, G. A. A. A. (2013). *Influence of substrate temperature on the structural, optical and electrical properties of CdS thin films deposited by thermal evaporation method*. Results in Physics, Vol. 3, pp. 173-178.
Ji, Z., He, Z., Song, Y., Liu, K., & Ye, Z. (2003). *Fabrication and characterization of indium doped p-type SnO_2 thin films*. Journal of Crystal growth, Vol. 259, pp. 282-285.
Ji, Z., Zhao, L., He, Z., Zhou, Q. & Chen, C. (2006). *Transparent p-type conductive indium-doped SnO_2 thin films deposited by spray pyrolysis*. Materials Letters, Vol. 60, pp. 1387-1389.
Joshi, B. N., Yoon H., & Yoon, S. S. (2013). *Structural, optical and electrical properties of tin oxide thin films by electrostatic spray* deposition. Journal of Electrostatics, Vol. 71, pp. 48-52.

Kim, H., Horwitz, J. S., Kushto, G., Pique, A., Kafafi, Z. H., Gilmore, C. M., & Chrisey, D. B. (2000). *Effect of film thickness on the properties of indium tin oxide thin films*. J. Appl. Phys., Vol. 88(10), pp. 6021-6025.

Mohammadi-Gheidari, A., SoleimaniAsl, E., Mansorhoseini, M., Mohajerzadeh, S., Madani, N., & Shams-Kolahi, W. (2005) *Structural properties of indium tin oxide thin films prepared for application in solar cells*. Mater Res. Bulletin, Vol. 40, pp. 1303-1307.

Mandal, M., Choudhury, S., Das., C. & Begum, T. (2014). *Substrate temperature dependent optical and structural properties of vacuum evaporated CdTe thin films*. European Scientific Journal, Vol. 10(3), pp. 442-455.

Pe Waal, H., & Simons, F. (1981). *Tin oxide coatings: Physical properties and applications*. Thin Solid Films, Vol. 77, pp. 253-258.

Roy, S. S., & Podder, J. (2010). *Synthesis and optical characterization of pure and Cu doped SnO_2 thin films deposited by spray pyrolysis*. Journal of Optoelectronics and Advanced Materials, Vol. 12(7), pp. 1479-1484.

Shamala, K. S., Murthy, L. C., & Narashimha Rao, K. (2004). *Studies on tin oxide films prepared by electron beam evaporation and spray pyrolysis method*. Bull. Mater. Sci., Vol. 27(3), pp. 295-301.

Tauc, J. (1974). *Amorphous and Liquid Semiconductors*. Plenum, London, pp. 159.

Tomlin, S. G. (1968). *Optical reflection and transmission formulae for thin films*. J. Phys. D: Appl. Phys, Vol. 1, pp. 1667-1671.

Tuna, O., Selamet, Y., Aygyn, G., & Ozyuzer, L. (2010). *High quality ITO thin films grown by dc and RF sputtering without oxygen*. J. Phys. D: Appl. Phys., Vol. 43, pp. 1-7.

Zadsar, M., Fallah, H. R., Hassanzadeh, M. H. A., & Varnamkhasti, M. G. (2012) *Substrate temperature effect on structural, optical and electrical properties of vacuum SnO_2 thin films*. Materials Science in Semiconductor Processing, Vol. 15, pp. 432-437.